

# Numerical simulations of the steady Navier–Stokes equations using adaptive meshing schemes

Lili Ju<sup>1</sup>, Hyung-Chun Lee<sup>2,\*</sup>,<sup>†</sup> and Li Tian<sup>1</sup>

<sup>1</sup>*Department of Mathematics, University of South Carolina, Columbia, SC 29208, U.S.A.*

<sup>2</sup>*Department of Mathematics, Ajou University, Suwon 443-749, Korea*

## SUMMARY

In this paper, we consider an adaptive meshing scheme for solution of the steady incompressible Navier–Stokes equations by finite element discretization. The mesh refinement and optimization are performed based on an algorithm that combines the so-called conforming centroidal Voronoi Delaunay triangulations (CfCVDTs) and residual-type local *a posteriori* error estimators. Numerical experiments in the two-dimensional space for various examples are presented with quadratic finite elements used for the velocity field and linear finite elements for the pressure. The results show that our meshing scheme can equally distribute the errors over all elements in some optimal way and keep the triangles very well shaped as well at all levels of refinement. In addition, the convergence rates achieved are close to the best obtainable. Extension of this approach to three-dimensional cases is also discussed and the main challenge is the efficient implementation of three-dimensional CfCVDT generation that is still under development. Copyright © 2007 John Wiley & Sons, Ltd.

Received 19 January 2007; Revised 8 May 2007; Accepted 14 May 2007

KEY WORDS: Navier–Stokes equations; centroidal Voronoi tessellation; conforming centroidal Voronoi Delaunay triangulations; *a posteriori* error estimators

## 1. INTRODUCTION

In many scientific and engineering problems, one always desires increasing the accuracy of the approximate solutions without adding unnecessary degrees of freedom. Therefore, adaptive algorithm have been playing more and more important roles in the solution process, that allows one to

\*Correspondence to: Hyung-Chun Lee, Department of Mathematics, Ajou University, Suwon 443-749, Korea.

<sup>†</sup>E-mail: hclee@ajou.ac.kr

Contract/grant sponsor: National Science Foundation; contract/grant number: DMS-0609575

Contract/grant sponsor: University of South Carolina Research and Productive Scholarship; contract/grant number: RPS-13060-06-12306

Contract/grant sponsor: KOSEF; contract/grant number: R01-2006-000-10472-0

refine the mesh in the critical regions while remaining reasonably coarse in the rest of the domain. Two important ingredients of adaptive algorithm for the numerical solution of partial differential equations (PDEs) are the local error estimator and the mesh adaptivity scheme, see [1–9] and references therein. Here, we are especially interested in the second ingredient. As pointed out in [10], for most current adaptive methods for PDEs, the meshes are only refined locally whenever some criterion based on a local error estimator is not satisfied on some elements; the mesh elsewhere in the domain is not changed. However, in an unrefined region, the errors could be so small that, because one has too many grid nodes there, computational resources are wasted.

Numerical solution of the Navier–Stokes equation has been one of central interests in the study of fluid mechanics in the past decades partially due to its many applications in various fields such as geophysics, atmospheric science, aerospace engineering and so on [11, 12]. In this paper, we propose an adaptive meshing scheme for numerical simulation of the steady incompressible Navier–Stokes equations (INSEs), that can distribute the nodes in some optimal way according to local *a posteriori* error estimates, so that the error of the resulting approximate solution is distributed equally over the elements. The key of our algorithm is the use of a meshing scheme called conforming centroidal Voronoi Delaunay triangulation (CfCVDT) [13]. A similar methodology for the solution of second-order linear elliptic PDEs was also proposed in [10]. Here our goal is to explore the effectiveness of such a methodology when applied to nonlinear problems such as the INSEs. The plan of the rest of the paper is as follows. We first give a short introduction to the steady INSE in the remaining of this section. In Section 2, we then discuss its finite element discretization and a specific local *a posteriori* error estimator. In Section 3, we propose our adaptive meshing scheme that connects the error estimators effectively with the CfCVDT mesh generator. In Section 4, several computational experiments in the two-dimensional space are carried out to demonstrate the high efficiency of our mesh adaptation approach. Finally, some conclusions are given in Section 5. We also would like to remark that we are currently studying the extension of this methodology to problems in three dimensions.

### 1.1. Steady incompressible Navier–Stokes equations

Let us consider the model steady Navier–Stokes equations for incompressible flows in a bounded and connected region  $\Omega$  in  $\mathbb{R}^d$ :

$$-\nu\Delta\mathbf{u} + (\mathbf{u} \cdot \nabla)\mathbf{u} + \nabla p = \mathbf{f} \quad \text{in } \Omega \quad (1)$$

$$\nabla \cdot \mathbf{u} = 0 \quad \text{in } \Omega \quad (2)$$

with boundary conditions

$$\mathbf{u} = \mathbf{g} \quad \text{on } \Gamma_D \quad \text{and} \quad (\mathbf{n} \cdot \nabla)\mathbf{u} = \mathbf{h} \quad \text{on } \Gamma_N \quad (3)$$

where  $\mathbf{u} \in \mathbb{R}^d$  represents the velocity and  $p \in \mathbb{R}$  the pressure, and  $\nu$  is the kinetic viscosity constant. The computational domain  $\partial\Omega = \Gamma_D \cup \Gamma_N$  where the Dirichlet boundary  $\Gamma_D$  must have positive measure and the Neumann part  $\Gamma_N$  can be empty. The functions  $\mathbf{g} \in \mathbf{H}^{1/2}(\Gamma_D)$  and  $\mathbf{h} \in \mathbf{H}^{-1/2}(\Gamma_N)$  are given. For the pure Dirichlet boundary value problem ( $\Gamma_N = \emptyset$ ), the boundary condition satisfies the following constraint:

$$\oint_{\partial\Omega} \mathbf{u} \cdot \mathbf{n} \, ds = 0 \quad (4)$$

where  $\mathbf{n}$  is the outer normal of  $\partial\Omega$ . Let us use the standard notation of Sobolev spaces and set

$$\mathbf{H}_D^1(\Omega) = (H_D^1(\Omega))^d \quad \text{and} \quad \mathbf{V} = \mathbf{H}_D^1(\Omega) \times L_0^2(\Omega)$$

where  $\mathbf{H}_D^1(\Omega) = \{\mathbf{u} \in \mathbf{H}^1(\Omega) \mid \mathbf{u} = \mathbf{0} \text{ on } \Gamma_D\}$  and  $L_0^2(\Omega) = \{q \in L^2(\Omega) \mid \int_{\Omega} q \, dx = 0\}$ . We will use the same notation for the corresponding norm on  $\mathbf{H}^1(\Omega)$  and  $L^2(\Omega)$ . Then define the following linear, bilinear, and trilinear functionals:

$$\begin{aligned} a : \mathbf{H}_D^1(\Omega) \times \mathbf{H}_D^1(\Omega) &\rightarrow \mathbb{R}, & a(\mathbf{u}, \mathbf{v}) &= \int_{\Omega} \nu \nabla \mathbf{u} \cdot \nabla \mathbf{v} \, dx \\ b : \mathbf{H}_D^1(\Omega) \times \mathbf{H}_D^1(\Omega) \times \mathbf{H}_D^1(\Omega) &\rightarrow \mathbb{R}, & b(\mathbf{u}, \mathbf{v}, \mathbf{w}) &= \int_{\Omega} (\mathbf{u} \cdot \nabla) \mathbf{v} \cdot \mathbf{w} \, dx \\ c : L_0^2(\Omega) \times \mathbf{H}_D^1(\Omega) &\rightarrow \mathbb{R}, & c(p, \mathbf{v}) &= \int_{\Omega} p \nabla \cdot \mathbf{v} \, dx \\ f : \mathbf{H}^{-1}(\Omega) &\rightarrow \mathbb{R}, & f(\mathbf{v}) &= \int_{\Omega} \mathbf{f} \cdot \mathbf{v} \, dx \end{aligned}$$

The forms  $a(\cdot, \cdot)$ ,  $c(\cdot, \cdot)$  and  $f(\cdot)$  are continuous and  $c(\cdot, \cdot)$  satisfies the standard inf–sup condition [4, 6]. The trilinear form  $b(\cdot, \cdot, \cdot)$  is also continuous and satisfies

$$\|b\| = \sup_{\mathbf{u}, \mathbf{v}, \mathbf{w} \in \mathbf{H}^1(\Omega)} \frac{b(\mathbf{u}, \mathbf{v}, \mathbf{w})}{|\mathbf{u}|_{1,\Omega} |\mathbf{v}|_{1,\Omega} |\mathbf{w}|_{1,\Omega}} < \infty$$

Then the standard weak form of Equations (1) and (2) is given by: find  $(\mathbf{u}, p) \in \mathbf{V}$  such that

$$\mathcal{L}((\mathbf{u}, p), (\mathbf{v}, q)) = f(\mathbf{v}) \quad \forall (\mathbf{v}, q) \in \mathbf{V} \quad (5)$$

where

$$\mathcal{L}((\mathbf{u}, p), (\mathbf{v}, q)) = a(\mathbf{u}, \mathbf{v}) + b(\mathbf{u}, \mathbf{u}, \mathbf{v}) - c(p, \mathbf{v}) - c(q, \mathbf{u}) \quad (6)$$

Due to Temam's work [11], a stabilization term is often added into  $b(\cdot, \cdot, \cdot)$  such that

$$b(\mathbf{u}, \mathbf{v}, \mathbf{w}) = \int_{\Omega} (\mathbf{u} \cdot \nabla) \mathbf{v} \cdot \mathbf{w} + \frac{1}{2} (\nabla \cdot \mathbf{u}) \mathbf{v} \cdot \mathbf{w} \, dx$$

Note that the above  $b(\mathbf{u}, \mathbf{v}, \mathbf{v}) = 0$  for all  $\mathbf{u}, \mathbf{v} \in \mathbf{H}_D^1(\Omega)$  and this modification will not affect the solution of problem (5).

In the following, we will also assume that the body force  $\mathbf{f}$  belongs to  $\mathbf{H}^{-1}(\Omega)$  and its norm is given by

$$\|\mathbf{f}\|_{-1,\Omega} = \sup_{\mathbf{v} \in \mathbf{H}^1(\Omega), \mathbf{v} \neq \mathbf{0}} \frac{f(\mathbf{v})}{|\mathbf{v}|_{1,\Omega}}$$

Then we have the following results about the existence and uniqueness of problem (5), see [6].

*Theorem 1*

Let  $\Omega$  be a bounded Lipschitz domain in  $\mathbb{R}^d$  ( $d \leq 3$ ) and  $\mathbf{f} \in \mathbf{H}^{-1}(\Omega)$ . Then there exists at least one solution  $(\mathbf{u}, p) \in \mathbf{V}$  to the problem (5). Moreover, if  $\|\mathbf{f}\|_{-1,\Omega} \leq v^2/\|b\|$ , then the solution  $(\mathbf{u}, p) \in \mathbf{V}$  is unique.

2. FINITE ELEMENT APPROXIMATION OF THE INSEs

In the following section, we will introduce in brief finite element approximations of Equation (5) and corresponding error estimates that will be used for our adaptive solution process.

2.1. Discretization and a priori error estimates

Let  $\Omega \in \mathbb{R}^d$  ( $d \leq 3$ ) be a bounded Lipschitz domain and  $\mathcal{T} = \{T_j\}$  be a conforming triangulation of  $\Omega$  ( $T_j$  are triangles for  $d = 2$  or tetrahedra for  $d = 3$ ). Denote by  $h_T$  the diameter of the element  $T \in \mathcal{T}$  and by  $r_T$  the diameter of the largest sphere that can be inscribed in  $T$ . We also assume that  $\mathcal{T}$  is regular, i.e. there is a constant  $\kappa > 0$  such that the ratio

$$\kappa_T = \frac{h_T}{r_T} \leq \kappa$$

for all  $T \in \mathcal{T}$ . Denote by  $\mathbb{P}_k$  the space of polynomials of degree  $\leq k$ . Let us choose the following finite element spaces:

$$\begin{aligned} \mathbf{Y}^h &= \{\mathbf{v}^h \in (C(\bar{\Omega}))^d \mid \mathbf{v}^h|_{T_j} \in (\mathbb{P}_{k+1}(T_j))^d, \forall T_j \in \mathcal{T}\} \\ \mathbf{X}^h &= \{\mathbf{v}^h \in \mathbf{Y}^h \mid \mathbf{v}^h|_{\partial\Omega} = \mathbf{0}\} \\ M^h &= \{q^h \in C(\bar{\Omega}) \mid q^h|_{T_j} \in \mathbb{P}_k(T_j), \forall T_j \in \mathcal{T}\} \\ Q^h &= \left\{ q^h \in M^h \mid \int_{\Omega} q^h \, dx = 0 \right\} \end{aligned} \tag{7}$$

and let  $\mathbf{V}^h = \mathbf{X}^h \times Q^h$  be the pair of discrete spaces for the velocity field and the pressure, respectively. For any  $(\mathbf{u}, p) \in \mathbf{V}$ , let us define

$$|(\mathbf{u}, p)|_V = (|\mathbf{u}|_{1,\Omega}^2 + v^{-2}|p|_{0,\Omega}^2)^{1/2} \tag{8}$$

Then, a finite element discretization for problem (5) have the following formulation: find  $(\mathbf{u}^h, p^h) \in \mathbf{V}^h$  such that

$$\mathcal{L}((\mathbf{u}^h, p^h), (\mathbf{v}^h, q^h)) = f(\mathbf{v}^h) \quad \forall (\mathbf{v}^h, q^h) \in \mathbf{V}^h \tag{9}$$

Problem (9) gives us a nonlinear system. In the case  $k = 1$  it bears the name of the Hood–Taylor discretization. See Figure 1 for a description of P2–P1 Hood–Taylor element in the two-dimensional space.

Under reasonable conditions, the following *a priori* error estimates can be established for the solution of discretization (9), see [6, 12].

*Theorem 2*

Let  $\Omega$  be a bounded Lipschitz domain in  $\mathbb{R}^d$  ( $d \leq 3$ ) and  $\mathbf{f} \in \mathbf{H}^{-1}(\Omega)$ . Let  $(\mathbf{u}, p)$  be the solution of problem (5). Then for  $v$  sufficiently large, there exists an  $h^*$  such that for all  $h \leq h^*$ , problem (9) has

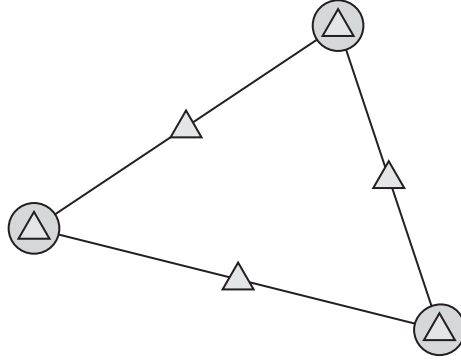


Figure 1. P2–P1 Hood–Taylor finite element where the triangles are the velocity nodes and the circles are the pressure nodes.

a unique solution  $(\mathbf{u}^h, p^h) \in \mathbf{V}^h$ . In addition, if  $(\mathbf{u}, p) \in (\mathbf{H}^{k+2}(\Omega) \cap \mathbf{H}_D^1(\Omega)) \times (H^{k+1}(\Omega) \cap Q(\Omega))$  where  $Q(\Omega) = \{q \in C(\bar{\Omega}) \mid \int_{\Omega} q \, dx = 0\}$ , then there exists a constant  $c$  independent of  $h$ , such that

$$|(\mathbf{u} - \mathbf{u}^h, p - p^h)|_V \leq ch^{k+1} \quad (10)$$

## 2.2. A posteriori error estimates

A priori estimates often do not play an important role in adaptive algorithms since configurations of exact solutions are generally not clear. In this paper, we will make use of a residual-based *a posteriori* error estimator for mesh refinement and optimization in our method.

Let  $\mathcal{E}_I$  denote the set of interior edges (or faces) of  $\mathcal{T}$ . If two elements  $T$  and  $T'$  of  $\mathcal{T}$  share the common edge (face)  $\gamma \in \mathcal{E}_I$ , define the jump in the normal flux of  $\mathbf{u}^h$  across the edge  $\gamma$  by

$$[(v\nabla\mathbf{u}^h) \cdot \mathbf{n}_\gamma]_\gamma = (v\nabla\mathbf{u}^h)|_T \cdot \mathbf{n}_T + (v\nabla\mathbf{u}^h)|_{T'} \cdot \mathbf{n}_{T'}$$

where  $\mathbf{n}_T$  is the unit outward normal vector to  $\partial T$ . Now set

$$\mathbf{r}_\gamma = \begin{cases} [(v\nabla\mathbf{u}^h) \cdot \mathbf{n}_\gamma]_\gamma & \text{if } \gamma \in \mathcal{E}_I \\ 0 & \text{if } \gamma \in \partial\Omega \end{cases} \quad (11)$$

and

$$\mathbf{R} = \mathbf{f} + v\Delta\mathbf{u}^h - (\mathbf{u}^h\nabla)\mathbf{u}^h - \frac{1}{2}(\nabla \cdot \mathbf{u}^h)\mathbf{u}^h - \nabla p^h \quad (12)$$

Then for any  $T \in \mathcal{T}$ , a local *a posteriori* error estimator on  $T$  proposed in [4] is defined by

$$\eta_T = \left[ |T| \|\mathbf{R}\|_{0,T}^2 + v^2 \|\nabla \cdot \mathbf{u}^h\|_{0,T}^2 + \frac{1}{2} \sum_{\gamma \in \partial T} |\gamma| \|\mathbf{r}_\gamma\|_{0,\gamma}^2 \right]^{1/2} \quad (13)$$

where  $|T|$  denotes the area (or volume) of  $T$  and  $|\gamma|$  the length (or area) of  $\gamma$ .

A local error estimator is called *reliable* if the true error can be bounded from above in terms of the local error estimator, and *efficient* if the true error is also locally bounded from below in term of the local error estimator. The following result for  $\eta_T$  has been proved in [4].

*Theorem 3*

For  $v$  sufficiently large, the local error estimator  $\eta_T$  defined in (13) is reliable for the Hood–Taylor discretization ( $d = 2$  and  $k = 1$  for  $\mathbf{X}^h$  and  $Q^h$  defined in (7)), i.e. there exists some constant  $c$  independent of  $h$ , such that

$$|(\mathbf{u} - \mathbf{u}^h, p - p^h)|_V \leq c\eta \tag{14}$$

where  $\eta = (\sum_{T \in \mathcal{T}} \eta_T^2)^{1/2}$ .

There is still no proof for the efficiency of the  $\eta_T$  yet, but it has been shown to be numerically very effective, see [4]. This local *a posteriori* estimator will be one of the two essential ingredients used for mesh refinement and optimization in our adaptive algorithm. Note that  $\eta_T$  is well defined with a given discrete solution  $(\mathbf{u}^h, p^h)$  for either two- or three-dimensional problems although Theorem 3 only holds for  $d = 2$ .

*Remark 1*

Many other good *a posteriori* error estimators also can be used here, such as the ones proposed in [6, 9]. All we need is an accurate local error indicator for the adaptive mesh construction although only this  $\eta_T$  defined in (13) is used for our numerical experiments in the paper.

### 3. ADAPTIVE MESHING SCHEME

Another essential ingredient of our adaptive method is a special meshing methodology, called *centroidal Voronoi tessellation* (CVT) proposed in [14], that can effectively control the local mesh sizes by pre-defining some density (nodes distribution) function.

#### 3.1. Conforming centroidal Voronoi Delaunay triangulations

Given an open bounded domain  $\Omega \in \mathbb{R}^d$  and a set of distinct points  $\{\mathbf{x}_i\}_{i=1}^n \subset \Omega$ . For each point  $\mathbf{x}_i, i = 1, \dots, n$ , define the corresponding Voronoi region  $V_i, i = 1, \dots, n$ , by

$$V_i = \{\mathbf{x} \in \Omega \mid \|\mathbf{x} - \mathbf{x}_i\| < \|\mathbf{x} - \mathbf{x}_j\| \text{ for } j = 1, \dots, n \text{ and } j \neq i\}$$

where  $\|\cdot\|$  denotes the Euclidean distance in  $\mathbb{R}^d$ . Clearly  $V_i \cap V_j = \emptyset$  for  $i \neq j$ , and  $\bigcup_{i=1}^n \bar{V}_i = \Omega$  so that  $\{V_i\}_{i=1}^n$  is a tessellation of  $\Omega$ . We refer to  $\{V_i\}_{i=1}^n$  as the *Voronoi tessellation* (VT) of  $\Omega$  associated with the point set  $\{\mathbf{x}_i\}_{i=1}^n$ . A point  $\mathbf{x}_i$  is called a *generator*; a subdomain  $V_i \subset \Omega$  is referred to as the *Voronoi region* corresponding to the generator  $\mathbf{x}_i$ . It is well known that the dual tessellation (in a graph-theoretical sense) to a Voronoi tessellation of  $\Omega$  is the so-called *Delaunay triangulation* (DT).

Given a density function  $\rho(\mathbf{x}) \geq 0$  defined on  $\Omega$ , for any region  $V \subset \Omega$ , define  $\mathbf{x}^*$ , the *centroid* of  $V$  by

$$\mathbf{x}^* = \frac{\int_V \mathbf{y} \rho(\mathbf{y}) \, d\mathbf{y}}{\int_V \rho(\mathbf{y}) \, d\mathbf{y}} \tag{15}$$

Then we refer to a Voronoi tessellation  $\{(\mathbf{x}_i, V_i)\}_{i=1}^n$  of  $\Omega$  as a CVT if and only if the points  $\{\mathbf{x}_i\}_{i=1}^n$  which serve as the generators of the associated Voronoi regions  $\{V_i\}_{i=1}^n$  are also the centroids of

those regions, i.e. if and only if we have that  $\mathbf{x}_i = \mathbf{x}_i^*$  for  $i = 1, \dots, n$ . The corresponding Delaunay triangulation is then called a *centroidal Voronoi Delaunay triangulation* (CVDT). CVTs are very useful in many applications, see [14] for details.

CVT and its dual CVDT-based methods have attracted a lot of attention in the area of high-quality mesh generation and optimization, see [15–17]. When CVT/CVDT is applied to numerical solution of PDEs, e.g. in a finite element method or finite volume method, some modifications are needed to handle geometric constraints. An obvious one is that the CVT/CVDT mesh must conform with the boundary of the target domain  $\Omega$ . Recently, a clear characterization of the influence of geometric constraints on the CVT-based meshing was proposed in [13]. Let us assume that the domain  $\Omega$  is compact and  $\partial\Omega$  is piecewise smooth with singular points  $P_S = \{\mathbf{z}_i\}_{i=1}^k$ . Denote by  $\mathbf{proj}(\mathbf{x})$  the process that projects  $\mathbf{x} \in \Omega$  to the point on the boundary closest to  $\mathbf{x}$ . Denote by  $P_I$  the set of generators whose Voronoi regions are interior and by  $P_B$  the set of generators whose Voronoi regions extend to the boundary, i.e.  $P_I = \{\mathbf{x}_i \mid \bar{V}_i \cap \partial\Omega = \emptyset\}$  and  $P_B = \{\mathbf{x}_i \mid V_i \cap \partial\Omega \neq \emptyset\}$ . Then a Voronoi tessellation  $\{(\mathbf{x}_i, V_i)\}_{i=1}^n$  of  $\Omega$  is called a CfcVT if and only if the following properties are satisfied:

- $P_S \subset \{\mathbf{x}_i\}_{i=1}^n$ ;
- $\mathbf{x}_i = \mathbf{x}_i^*$  if  $\mathbf{x}_i \in P_I$ ;
- $\mathbf{x}_i = \mathbf{proj}(\mathbf{x}_i^*)$  if  $\mathbf{x}_i \in P_B - P_S$ .

The corresponding triangulation is called a CfcCVDT. Some efficient techniques for the construction of CfcCVDTs in the two-dimensional space were proposed and implemented using the so-called *constrained Delaunay triangulation* (CDT) process and a modified Lloyd-type algorithm, see [13–16] for details. Many sample CfcCVDT meshes are also given in [13]. The three-dimensional implementation is still under development. Some other techniques for constructing CVT-based triangulations can be found in [16, 17]. An important and very useful conjecture for CVT/CVDT-based (or CfcCVDT) meshes is that

$$\frac{h_i}{h_j} \approx \left( \frac{\rho(\mathbf{x}_j)}{\rho(\mathbf{x}_i)} \right)^{1/(d+2)} \quad (16)$$

where  $h_i$  denotes the diameter of the Voronoi cell  $V_i$ . This asymptotic relation has been rigorously proven to be true in the one-dimensional space [14]. Although still remaining to be only a conjecture in higher dimensional spaces, it has been verified numerically by many experiments and is widely assumed in practical applications such as vector quantization and image processing [18].

The CfcCVDT meshes have been successfully used in [10] for adaptive computations of numerical solution of linear second-order elliptic PDEs. The main idea of our adaptive meshing algorithm for the solution of the steady INSE (1) is similar to the one taken in [10], i.e. to refine the old mesh and then optimize (or say re-mesh) it based on CfcVDT algorithms according to some density function. A major advantage of this approach is that we may determine a density function  $\rho$  based on some posteriori error estimator and to generate the new mesh so that the errors of the new approximate solution will be equally distributed over the elements in an optimal way (i.e. with respect to the number of mesh nodes). Another advantage of this approach is that the resulting mesh always has good quality due to CVT's properties described above while most adaptive methods often deteriorate the mesh quality along the refinements.

### 3.2. Determination of the density function

Assume that we use the *a posteriori* error estimator  $\eta_T$  defined in (13) for the adaptive meshing. An important question then is how to determine a proper density function for the new CfVDT mesh  $\mathcal{T}^{(\ell+1)}$  at the refinement level  $(\ell + 1)$  based on the local error estimator  $\eta_T^{(\ell)}$  of the approximate solution at the previous mesh  $\mathcal{T}^{(\ell)}$ . A similar technique to that suggested in [10] can be derived. The basic idea is to construct a density function  $\rho^{(\ell+1)}$  to adjust the local mesh size so that  $\eta_T^{(\ell+1)}$  will be equally distributed as much as possible on each triangle  $T \in \mathcal{T}^{(\ell+1)}$ .

Let us define on each triangle  $T \in \mathcal{T}^{(\ell)}$

$$\tilde{\rho}_T = \frac{(\eta_T^{(\ell)})^{(d+2)/(k+2)}}{h_T^{d+2}}$$

We then uniquely determine a piecewise linear function  $\rho^{(\ell+1)}$  (with respect to  $\mathcal{T}^{(\ell)}$ ) such that for any vertex  $\mathbf{x}_i$  of  $\mathcal{T}^{(\ell)}$ ,

$$\rho^{(\ell+1)}(\mathbf{x}_i) = \frac{\sum_{T \in S_i} \tilde{\rho}_T}{\text{card}(S_i)} \quad (17)$$

where  $S_i = \{T \in \mathcal{T}^{(\ell)} \mid \mathbf{x}_i \in \bar{T}\}$ . Note that, if the local error estimator  $\eta_T$  and *a priori* estimate (10) are really good approximations to the true error locally (i.e. inequality (14) in Theorem 3 holds for general  $d$  and  $k$ ), then we may assume that, there exists a constant  $c_T$ , depending on the position of  $T$  in the domain  $\Omega$ , but independent of the size of  $T$ , such that

$$\eta_T^2 \approx c_T h_T^{2(k+1)+d} \quad (18)$$

Relation (18) is then obtained by comparing *a priori* error estimate (10) with (14). Combining (18) with the CVT/CVDT property (16), it is not difficult to verify that the CfCVDT mesh  $\mathcal{T}^{(\ell+1)}$  generated by the density function  $\rho^{(\ell+1)}$  will approximately have the property that

$$\eta_{T_i}^{(\ell+1)} \approx \eta_{T_j}^{(\ell+1)}$$

for any elements  $T_i, T_j \in \mathcal{T}^{(\ell+1)}$ . We like to point out that the density function  $\rho^{(\ell+1)}$  defined through (17) may not be an optimal choice if (14) does not hold, and it also can be applied to other type of local *a posteriori* error estimators satisfying Theorems 2 and 3.

The most time consuming step in the calculations of  $\rho^{(\ell+1)}$  is the nearest neighbour search operation since they are defined by interpolation with respect to an unstructured mesh. However, this task can be efficiently solved using the software package ‘ANN’ [19] as suggested in [10].

#### Remark 2

For the INSE in a two-dimensional domain ( $d = 2$ ), if the Hood–Taylor discretization is used, then we especially have

$$\tilde{\rho}_T = \frac{(\eta_T^{(\ell)})^{4/3}}{h_T^4} \quad (19)$$

*Remark 3*

The discussion above may not be applied to the cases in which the solution has strong anisotropy. See the discussion given in [10].

3.3. Adaptive algorithm

Let  $\mathcal{E}^{(\ell)} = \{E_i\}_{i=1}^{k^{(\ell)}}$  denote the set of edges of the  $\ell$ th level triangulation  $\mathcal{T}^{(\ell)}$  and  $k^{(\ell)}$  be the number of elements of  $\mathcal{E}^{(\ell)}$ . Set  $\rho_{E_i} = \rho(\mathbf{y}_i)$  for any density function  $\rho$ , where  $\mathbf{y}_i$  denotes the mid-point of the edge  $E_i$ . Let  $CfCVD T(\mathcal{T}, \Omega, \rho)$  denote the construction algorithm for CfCVD T meshes taking  $\mathcal{T}$  as the initial configuration for  $\Omega$  and  $\rho$  as the density function. We can now define our adaptive meshing algorithm similar to the one used in [10] but with slight difference as follows.

*Algorithm 1*

Given a domain  $\Omega$ , an integer  $N_{\max} > 0$ , an integer  $L_{\max}$ , and a parameter  $0 < \theta \leq 1$ .

0. Generate an initial coarse triangulation  $\mathcal{T}^{(0)}$  of  $\Omega$ . Let  $n^{(0)}$  denote the number of vertices of  $\mathcal{T}^{(0)}$  and set  $\ell = 0$ .
1. Solve the INSE using the finite element method on  $\mathcal{T}^{(\ell)}$ . If  $\ell > L_{\max}$  or  $n^{(\ell)} > N_{\max}$ , terminate; otherwise, go to step 2.
2. Determine the local error estimator  $\eta_T^{(\ell)}$  for all  $T \in \mathcal{T}^{(\ell)}$ .
3. Construct  $\rho^{(\ell+1)}$  using (17) and set the density function  $\rho = \rho^{(\ell+1)}$ . Determine  $\{\rho_{E_i}\}_{i=1}^{k^{(\ell)}}$  and sort them in decreasing order.
4. Add  $\{\mathbf{y}_i\}_{i=1}^{k_\theta}$  into the triangulation  $\mathcal{T}^{(\ell)}$ , where

$$k_\theta = \max \left\{ k^* \left| \sum_{i=1}^{k^*} \rho_{E_i} < \theta \sum_{i=1}^{k^{(\ell)}} \rho_{E_i} \right. \right\}$$

and then form the new intermediate triangulation  $\tilde{\mathcal{T}}^{(\ell+1)}$  with  $n^{(\ell+1)} = n^{(\ell)} + k_\theta$  vertices.

5. Optimize  $\tilde{\mathcal{T}}^{(\ell+1)}$  to obtain  $\mathcal{T}^{(\ell+1)} = CfCVD T(\tilde{\mathcal{T}}^{(\ell+1)}, \Omega, \rho)$ , set  $\ell \leftarrow \ell + 1$ , then go to step 1.

The parameter  $\theta$  in Algorithm 1 is used here to control the refinement process. The sorting procedure in step 4 can be implemented efficiently using a quick sorting algorithm. This algorithm is slightly different with the one presented in [10] for which a pre-processing step is used to obtain a good initial mesh. We think such a pre-processing is not very helpful in improving quality of the resulting adaptive meshes since the refined meshes will move at each level according to some density functions.

*Remark 4*

This adaptive meshing scheme for INSEs also can be adapted to other discretizations and local *a posteriori* error estimators with appropriate changes on density functions.

*Remark 5*

The marking strategy based on the parameter  $\theta$  used in this adaptive algorithm is due to Dörfler [1]. It ensures that we choose sufficiently many edges such that their contributions constitute a fixed

proportion of the global error estimator. In most existing adaptive methods, the smaller  $\theta$  is, the more optimal the resulting adaptive meshes are (in the sense of error reduction vs the number of nodes), but it also requires more levels of mesh refinement and solution process to reach some pre-defined error threshold since less new nodes will be added into the old mesh at each level. The selection of  $\theta$  in practical applications is often a trade-off of these two issues in order to obtain to good efficiency (with respect to time) of the adaptive algorithm. For detailed discussions, see [1, 7, 8]. It is worth noting that due to the extra optimization step we may choose a relative larger  $\theta$  for our adaptive Algorithm 1 while the resulting meshes are still quite optimal.

#### 4. NUMERICAL EXPERIMENTS

In our numerical simulations, we only consider the two-dimensional space and the Hood–Taylor scheme is used for the discretization of the INSEs (1) and (2). The CfCVDT mesh generator in [13] is used, which is implemented based on the ‘*Triangle*’ package [20]. The resulting nonlinear system (9) after discretization is solved by Newton’s method.

We set  $\theta = 0.3$  for all test problems (this is an experience number). For our adaptive methods, the convergence rate CR with respect to the norm  $\|\cdot\|$  at the refinement level  $\ell$  is roughly computed by

$$\text{CR} = \frac{2 \log(\|e_{h,\ell}\|/\|e_{h,\ell-1}\|)}{\log(n_{\ell-1}/n_{\ell})} \quad (20)$$

where  $n_{\ell}$  denotes the number of nodes and  $\|e_{h,\ell}\|$  denotes the error  $\|(\mathbf{u} - \mathbf{u}^h, p - p^h)\|_V$  at the refinement level  $\ell$  or the global error estimator  $\eta^{(\ell)}$  if the exact solution  $(\mathbf{u}, p)$  is unknown. In order to evaluate the distribution of the local error estimator  $\eta_T$  over all elements of  $\mathcal{T}$ , we define the normalized standard deviation  $\text{STD}_{\eta_T}$  by

$$\text{STD}_{\eta_T} = \frac{\sqrt{\sum_{T \in \mathcal{T}} (\eta_T - \mathbf{E}\eta)^2 / \text{card}(\mathcal{T})}}{\mathbf{E}\eta} \quad (21)$$

where  $\mathbf{E}\eta$  denotes the expectation of  $\eta_T$ , i.e.  $\mathbf{E}\eta = \sum_{T \in \mathcal{T}} \eta_T / \text{card}(\mathcal{T})$ .

We apply the commonly used  $q$  measure to evaluate the quality of triangular meshes, where for any triangle  $T$ ,  $q$  is defined to be twice the ratio of the radius  $R_T$  of the largest inscribed circle and the radius  $r_T$  of the smallest circumscribed circle, i.e.

$$q(T) = 2 \frac{R_T}{r_T} = \frac{(b+c-a)(c+a-b)(a+b-c)}{abc}$$

where  $a$ ,  $b$ , and  $c$  are side lengths of  $T$ . For a given triangulation  $\mathcal{T}$ , we define

$$q_{\min} = \min_{T \in \mathcal{T}} q(T) \quad \text{and} \quad q_{\text{avg}} = \frac{1}{\text{card}(\mathcal{T})} \sum_{T \in \mathcal{T}} q(T) \quad (22)$$

where  $q_{\min}$  will be used to measure the quality of the worst triangle and  $q_{\text{avg}}$  the average quality of the mesh  $\mathcal{T}$ .

#### 4.1. Back-step problem

The first problem we tested is the so-called back-step problem where the domain was chosen to be  $\Omega = ([-0.5, 9.5] \times [0, 0.5]) \cup ([0, 9.5] \times [-0.5, 0])$ . The boundary conditions were set to be

$$\mathbf{u}(x, y) = \begin{cases} (16y(0.5 - y), 0) & \text{on the inflow boundary } \Gamma_i = \{-0.5\} \times [0, 0.5] \\ (0, 0) & y = -0.5 \text{ or } y = 0.5 \text{ or } y = 0 \text{ \& } -0.5 \leq x \leq 0 \end{cases} \quad (23)$$

$$(\mathbf{u} \cdot \nabla) \mathbf{n} = 0 \quad \text{on the inflow boundary } \Gamma_o = \{9.5\} \times [-0.5, 0.5]$$

We also chose the body force  $\mathbf{f} = (0, 0)$  and the Reynolds number  $Re = 1/\nu = 800$ . It is known the exact solution  $(\mathbf{u}, p)$  for this problem is smooth, i.e.  $\mathbf{u} \in \mathbf{H}^3(\Omega)$  and  $p \in H^3(\Omega)$ , respectively. Since the exact solution is not obtainable, the convergence rate will be then computed based on the *a posteriori* error estimator  $\eta$  instead of the true error.

For this problem, we set  $N_{\max} = 10\,000$ . The initial mesh and repeatedly refined CfCVDT meshes at some levels generated using Algorithm 1 for the back-step problem are shown in Figure 2. The distributions of nodes in the CfCVDT-based adaptive meshing process clearly show the accumulation of nodes in the vicinity of the origin and a strip close to the middle part of the domain from left to right. Table I reports information about mesh quality, error estimators and convergence rates at all refinement levels for this problem. The values of  $q_{\min}$  and  $q_{\text{avg}}$  given in Table I demonstrate that the shape quality of the meshes resulting from the CfCVDT-based adaptive meshing strategy is always very good at all levels for the density functions  $\rho$  (17) defined based on the local *a posteriori* error estimator  $\eta_T$ , although the mesh sizes vary a lot over the  $\Omega$ , e.g.  $h_{\max}/h_{\min}$  reaches 36.66 at the last level. It is also interesting to observe  $h_{\max}/h_{\min}$  tends to monotonically increase for the adaptive methods. Figure 3 shows the distribution of the percentage of elements with different quality measures for the resulting CfCVDT mesh at the last refinement level. The mesh clearly tends to have larger concentration of elements in the group  $0.9 < q < 1$ . One also observes that our CfCVDT-based adaptive meshing method obtained very nice convergence rates (the theoretical perfect convergence rate is 2 according to Theorem 2) along the refinements although they are not very stable at the beginning of refinements and also deteriorate a little at the last several levels.

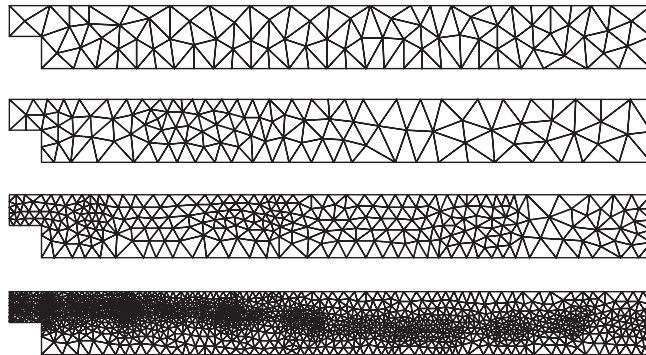


Figure 2. Adaptively refined meshes at some levels generated for the back-step problem. From top to bottom: initial mesh with 103 nodes and the CfCVDT meshes with 125, 301 and 1397 nodes, respectively.

Table I. Mesh quality, error estimators, and convergence rates for the back-step problem.

$\ell$	$n_\ell$	$q_{\min}$	$q_{\text{avg}}$	$h_{\min}$	$\frac{h_{\max}}{h_{\min}}$	$\eta$	CR	$\text{STD}_{\eta_T}$
0	103	0.492	0.865	2.40e-01	2.86	2.8732e-01	—	1.638
1	125	0.703	0.923	2.47e-01	2.73	3.0376e-01	-0.575	1.763
2	149	0.624	0.918	1.63e-01	4.66	1.7332e-01	6.390	1.630
3	183	0.666	0.932	1.63e-01	4.04	9.9454e-02	5.405	1.260
4	234	0.664	0.930	1.52e-01	3.71	7.1336e-02	2.703	1.498
5	301	0.655	0.931	1.10e-01	4.67	4.8571e-02	3.053	1.224
6	396	0.660	0.932	8.43e-02	5.43	4.4765e-02	0.595	1.324
7	522	0.709	0.936	6.85e-02	7.53	3.6459e-02	1.486	1.285
8	697	0.508	0.934	6.78e-02	5.96	2.1176e-02	3.759	0.987
9	971	0.618	0.939	5.22e-02	6.61	1.6014e-02	1.686	0.912
10	1397	0.653	0.944	3.97e-02	8.07	1.0422e-02	2.362	0.813
11	2048	0.555	0.939	3.16e-02	8.87	7.3557e-03	1.822	0.747
12	3036	0.601	0.943	2.49e-02	11.22	5.0480e-03	1.913	0.672
13	4609	0.550	0.942	1.41e-02	16.22	3.4516e-03	1.821	0.600
14	7106	0.607	0.943	7.17e-03	27.88	2.4270e-03	1.627	0.546
15	11 076	0.567	0.944	4.83e-03	36.66	1.7066e-03	1.687	0.485

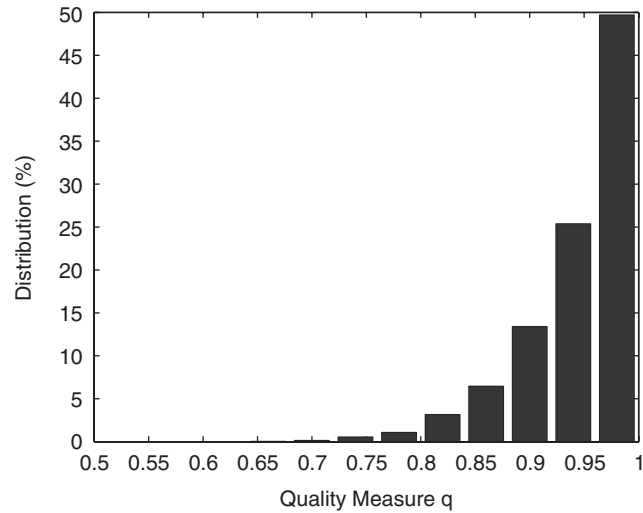


Figure 3. Distribution of the percentage of elements with different quality measures for the resulting CfCVDT mesh at the level 15 for the back-step problem.

An important optimal property of CfCVDT-based adaptive methods is the equal distribution of the errors over all elements of the mesh. In order to verify this, we also present the values of  $\text{STD}_{\eta_T}$  defined in (21) at all refinement levels in Table I. It is obvious that our adaptive meshing scheme does indeed distribute the errors more and more equally over all elements inflected by the

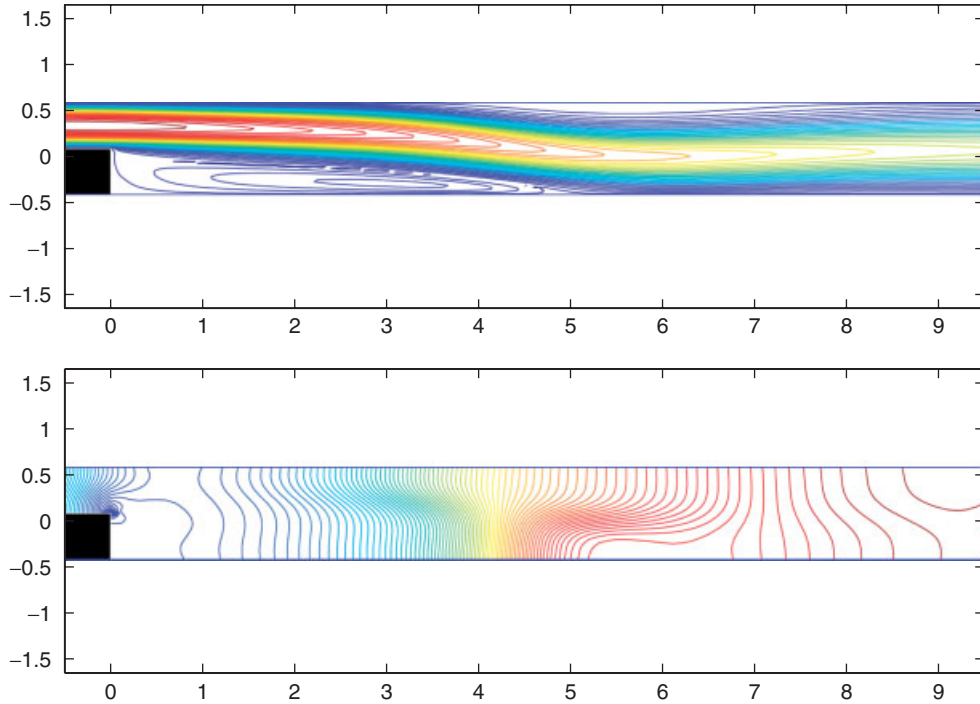


Figure 4. Plots of the approximate solution with 11 076 nodes for the back-step problem. Top: the magnitude of velocity field  $\mathbf{u}^h$ ; bottom: the pressure field  $p^h$ .

decreasing of  $\text{STD}_{\eta_T}$  along the refinements. Finally, the approximate velocity and pressure fields ( $\mathbf{u}^h$ ,  $p^h$ ) at the last refinement level are shown in Figure 4 for visualization purpose.

#### 4.2. Channel flow past a circular cylinder problem

The second problem we tested is the flow past a circular cylinder in a channel, abbreviated as the *cylinder* problem. Let a rectangle be given by  $\Omega_1 = [-2, 20] \times [-2, 2.1]$  and a circle by  $\Omega_2 = \{(x, y) \mid x^2 + y^2 < 0.5^2\}$ , the target domain is then set to be  $\Omega = \Omega_1 - \Omega_2$ . We would like to remark that  $\Omega$  is not symmetric with respect to the  $x$ -axis. The boundary condition is given by

$$\mathbf{u}(x, y) = \begin{cases} \left( \frac{(2+y)(2.1-y)}{4.2}, 0 \right) & \text{on the inflow boundary } \Gamma_i = \{-2.0\} \times [-2, 2.1] \\ (0, 0) & \text{on } \partial\Omega_2 \end{cases} \quad (24)$$

$$(\mathbf{u} \cdot \nabla) \mathbf{n} = 0 \quad \text{on the outflow boundary } \Gamma_o = \{20\} \times [-2, 2.1]$$

$$v = 0 \quad \text{and} \quad \frac{\partial u}{\partial x} = 0 \quad \text{on the top and bottom boundaries}$$

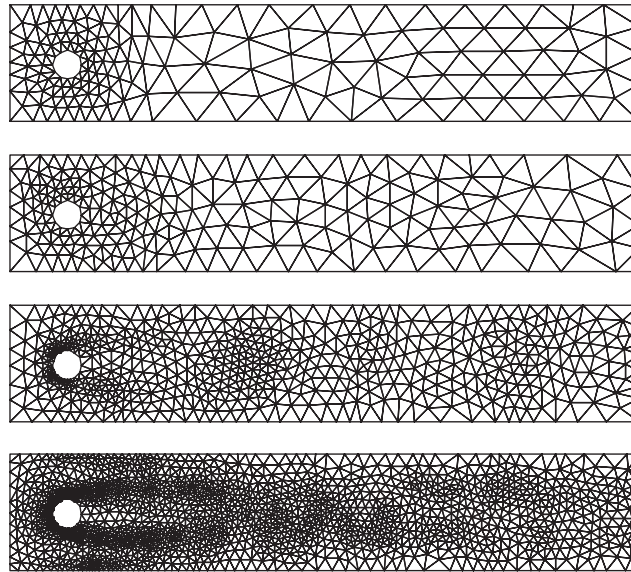


Figure 5. Adaptively refined meshes at some levels generated for cylinder problem. From top to bottom: initial mesh with 181 nodes and the CfCVDT meshes with 236, 645 and 1956 nodes, respectively.

where  $\mathbf{u} = (u, v)$ . We again let the body force  $\mathbf{f} = (0, 0)$  and the Reynolds number  $Re = 1/\nu = 200$  for this cylinder problem. It is well known that the solution  $(\mathbf{u}, p)$  for this problem is not globally smooth, i.e.  $\mathbf{u}$  and  $p$  only belong to  $\mathbf{H}^1(\Omega)$  and  $H^1(\Omega)$ , respectively, instead of  $\mathbf{H}^2(\Omega)$  and  $H^2(\Omega)$ .

For this problem, we again set  $N_{\max} = 10\,000$ . Due to the high sensitivity of the cylinder problem, we choose the initial mesh with more points concentrating around the cylinder to guarantee the convergence of Newton's iteration. Figure 5 displays refined meshes at some levels generated by our CfCVDT-based adaptive meshing method. The distributions of nodes in the CfCVDT-adapted meshes clearly show the heavy accumulation of nodes near the region close to the left side of the cylinder and the sparsity near its right side. Table II reports information about mesh quality, error estimators and convergence rates at all refinement levels for this cylinder problem. Again, all triangles are well shaped at all refinement levels, an observation that is supported by the values of  $q_{\min}$  and  $q_{\text{avg}}$  listed in Table II. At the same time, the values of  $h_{\max}/h_{\min}$  in Table II also shows the high variation of mesh sizes through the domain  $\Omega$ , that reach the maximum 74.99 at the last level. Notice that this value 74.99 here is more than twice bigger than the one for the back-step problem due to the singularity of the exact solution. The distribution of the percentage of elements with different quality measures of the resulting CfCVDT meshes for this example is very similar to the one presented in Figure 3 although not shown here due to the similarity.

Although  $\mathbf{u}$  and  $p$  are not smooth enough, the convergence rates obtained by our adaptive scheme are still as good as the ones for the back-step problem that has a smooth solution. From the values of  $\text{STD}_{\eta_T}$  list in Table II, it is again obvious that our CfCVDT-based adaptive meshing

NUMERICAL SIMULATIONS OF THE STEADY NAVIER–STOKES EQUATIONS

Table II. Mesh quality, error estimators, and convergence rates for the cylinder problem.

$\ell$	$n_\ell$	$q_{\min}$	$q_{\text{avg}}$	$h_{\min}$	$\frac{h_{\max}}{h_{\min}}$	$\eta$	CR	$\text{STD}_{\eta_T}$
0	181	0.477	0.876	2.30e−01	4.14	1.0590e+00	—	1.154
1	236	0.678	0.934	2.70e−01	7.09	9.0408e−01	1.192	1.133
2	333	0.429	0.931	1.96e−01	13.19	5.7878e−01	2.591	1.136
3	470	0.589	0.937	1.38e−01	16.25	4.3911e−01	1.603	1.181
4	645	0.632	0.937	8.98e−02	13.02	3.0286e−01	2.347	1.084
5	922	0.627	0.938	6.89e−02	16.00	2.0164e−01	2.277	0.969
6	1339	0.651	0.941	4.87e−02	23.44	1.2657e−01	2.496	0.935
7	1956	0.595	0.936	3.56e−02	25.70	8.7698e−02	1.936	0.823
8	2924	0.593	0.941	2.75e−02	26.74	5.8315e−02	2.029	0.705
9	4468	0.604	0.940	2.10e−02	38.97	4.0594e−02	1.709	0.660
10	6848	0.576	0.941	1.38e−02	53.84	2.8563e−02	1.646	0.588
11	10627	0.622	0.941	9.84e−03	74.99	2.0117e−02	1.596	0.537

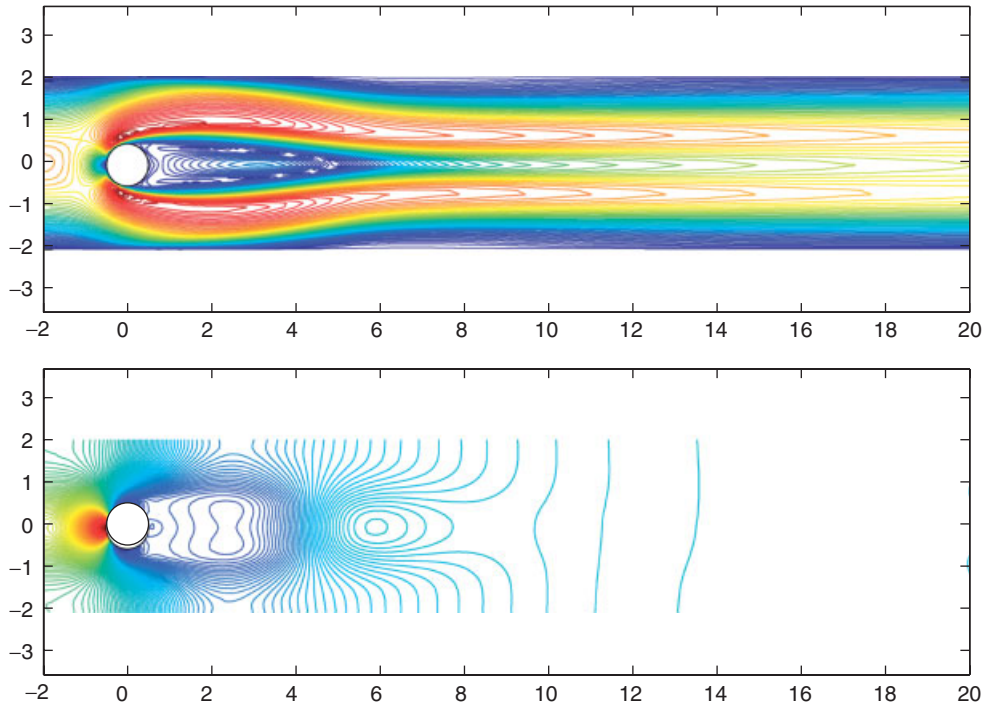


Figure 6. Plots of the approximate solution with 10 596 nodes for the cylinder problem. Top: the magnitude of velocity field  $\mathbf{u}^h$ ; bottom: the pressure field  $p^h$ .

method distributes the errors more and more equally over the triangles along the refinements. We finally display the representative approximate solution  $(\mathbf{u}^h, p^h)$  at the last refinement level in Figure 6 for visualization.

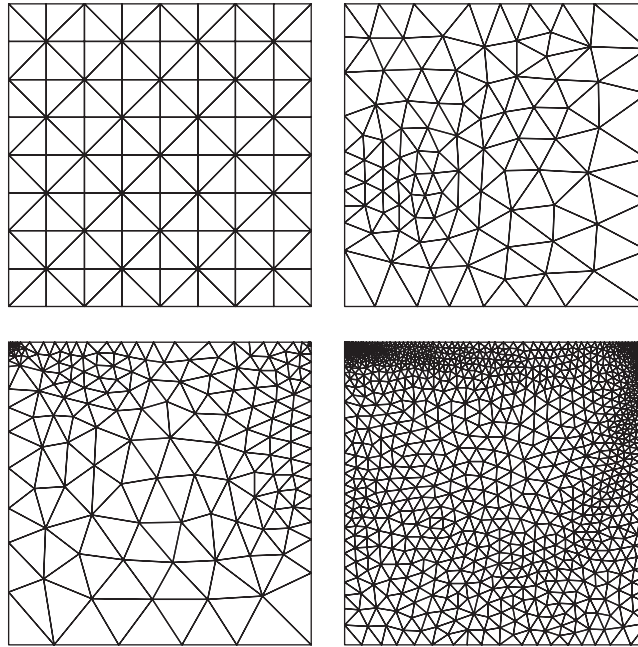


Figure 7. Adaptively refined meshes at some levels generated for the driven cavity problem. Top to bottom and left to right: initial mesh with 81 nodes and the CfcVDT meshes with 103, 193 and 1175 nodes, respectively.

#### 4.3. Driven cavity problem

The third problem we tested is the so-called driven cavity problem. Let the domain be a square given by  $\Omega = [-1, 1] \times [-1, 1]$  and set the pure Dirichlet boundary condition to be

$$\mathbf{u}(x, y) = \begin{cases} (1, 0), & [-1, 1] \times \{1\} \\ (0, 0), & \text{otherwise} \end{cases} \quad (25)$$

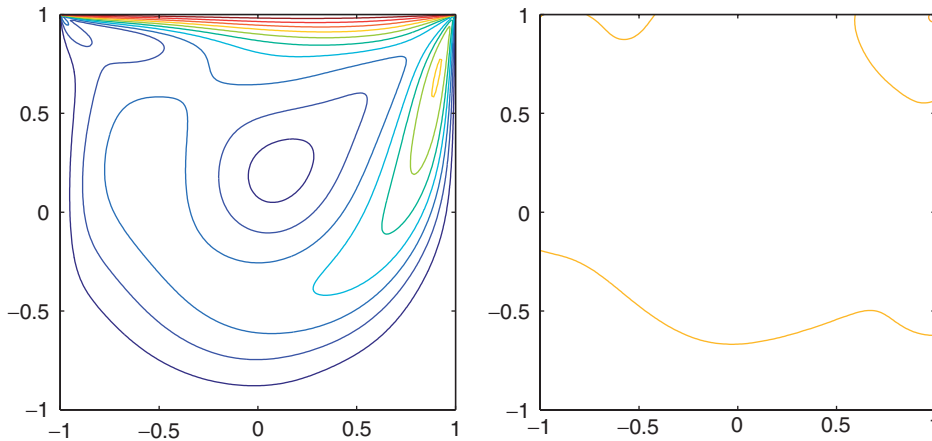
We also set the body force  $\mathbf{f} = (0, 0)$  and the Reynolds number  $Re = 1/\nu = 500$  for this problem. It is well known that the solution  $(\mathbf{u}, p)$  for this driven cavity problem satisfies  $\mathbf{u} \notin \mathbf{H}^1(\Omega)$  and  $p \notin H^1(\Omega)$ . Especially,  $\mathbf{u}$  and  $p$  have very strong singularity at the two top corners  $(-1, 1)$  and  $(1, 1)$  (it is easy to see that the velocity field  $\mathbf{u}$  jumps there) but are smooth elsewhere. It is worth pointing out that the discrete solution  $(\mathbf{u}^h, p^h)$  will converge to the exact solution  $(\mathbf{u}, p)$  only under the  $\mathbf{L}^2 \times L^2$  norm, but not under the  $\|\cdot\|_V$  norm. Consequently, the global error estimator  $\eta$  will not go to zero along the refinements. So we made the following changes to the local *a posteriori* error estimator  $\eta_T$  defined in (13):

$$\tilde{\eta}_T^2 = \eta_T^2 |T| \quad (26)$$

and  $\tilde{\eta} = (\sum_{T \in \mathcal{T}} \tilde{\eta}_T^2)^{1/2}$ . The above modification basically means that  $\tilde{\eta}_T$  will be used to estimate the error  $\|\mathbf{u} - \mathbf{u}^h\|_{0,\Omega} + \nu^{-2} \|p - p^h\|_{-1,\Omega}$  since the exact solution has less regularity. So it is more reasonable to use the  $\tilde{\eta}_T$  in (19) for the determination of the density function  $\rho$  instead of  $\eta_T$ .

Table III. Mesh quality, error estimators, and convergence rates for the driven cavity problem.

$\ell$	$n_\ell$	$q_{\min}$	$q_{\text{avg}}$	$h_{\min}$	$\frac{h_{\max}}{h_{\min}}$	$\tilde{\eta}$	CR	$\text{STD}_{\tilde{\eta}_T}$
0	81	0.828	0.828	1.76e−01	1.00	4.8359e+00	—	1.409
1	103	0.709	0.931	1.37e−01	3.93	1.0031e−01	32.258	1.486
2	125	0.491	0.911	1.46e−01	4.82	1.2828e−02	21.247	2.398
3	137	0.536	0.911	4.19e−02	16.25	8.5610e−03	8.823	1.807
4	155	0.558	0.909	1.44e−02	28.93	5.3056e−03	7.751	1.278
5	193	0.350	0.904	8.58e−03	57.45	3.3694e−03	4.141	0.980
6	249	0.274	0.901	7.10e−03	48.29	2.0454e−03	3.918	0.806
7	343	0.400	0.924	5.78e−03	42.23	1.1905e−03	3.379	0.594
8	505	0.586	0.936	5.37e−03	48.39	7.4202e−04	2.444	0.633
9	767	0.513	0.933	4.19e−03	62.43	4.4451e−04	2.452	0.620
10	1175	0.421	0.938	2.93e−03	61.29	2.8471e−04	2.088	0.677
11	1835	0.638	0.938	1.95e−03	88.11	1.6954e−04	2.326	0.612
12	2868	0.621	0.942	1.64e−03	76.24	1.3168e−04	1.132	1.072
13	4539	0.652	0.943	1.04e−03	145.50	6.7523e−05	2.910	0.708
14	5708	0.661	0.943	7.55e−04	160.31	5.9412e−05	1.117	0.664


 Figure 8. Plots of the approximate solution with 5708 nodes for the driven cavity problem. Left: the magnitude of velocity field  $\mathbf{u}^h$ ; right: the pressure field  $p^h$ .

For this problem, we set  $N_{\max} = 5000$  since the domain is much smaller compared with former problems. The initial mesh and repeatedly refined CfCVDT meshes at some levels generated for the driven cavity problem are shown in Figure 7. The distributions of nodes in the CfCVDT-based adaptive meshes clearly show the accumulation of nodes near the points  $(1, 1)$  and  $(-1, 1)$  where the singularities in the solution occur, especially the latter one. Table III contains information about mesh quality, solution errors, and convergence rates at all refinement levels for the driven cavity problem. One sees that the CfCVDT-based adaptive methods still achieve excellent convergence rates with respect to  $\tilde{\eta}$  although some instabilities show up at levels 12 and 14. Also, once again,

all triangles remain well shaped at all refinement levels, an observation that is supported by the values of  $q_{\min}$  and  $q_{\text{avg}}$  listed in Table III even though the mesh sizes vary greatly over the  $\Omega$ , e.g.  $h_{\max}/h_{\min}$  reaches 160.31 at the last level. Notice that the value 160.31 here is much bigger than that for the back-step problem and the cylinder problem due to the much stronger singularity. The distribution of the percentage of elements with different quality measures of the resulting CfCVDT meshes is again not shown here due to the similarity with Figure 3. The decrease of  $\text{STD}_{\tilde{\eta}_T}$  in III along the refinements again demonstrates the effectiveness of our adaptive meshing scheme in distributing the errors more and more equally over all elements. We also display the approximate solution  $(\mathbf{u}^h, p^h)$  at the last refinement level in Figure 8 for visualization purpose.

## 5. CONCLUSIONS

In this paper, we presented an efficient and robust adaptive mesh refining algorithm for solution of the steady incompressible Navier–Stokes equations using finite element approximations. Our meshing scheme combines *a posteriori* error estimation with the so-called CfCVDT. The two ingredients are well connected together by the fact that the density function required by the second one is defined and computed from the first one. Various numerical experiments in the two-dimensional space were carried out and showed that our meshing technique is very robust and obtained convergence rates (evaluated by the global *a posteriori* error estimate) close to the optimal one for the Hood–Taylor elements. An interesting question not addressed in this paper is the impact of our adaptive remeshing on the convergence properties of Newton’s part of the solution process and that would be one of our future research work. Our mesh adaptation strategy also can be easily generalized and applied to higher-order finite element approximations. Extension of this approach to three-dimensional cases is also natural, and the main challenge is the efficient implementation of three-dimensional CfCVDT mesh generation that is still under development. Existing tools such as the successor of ‘Triangle’ in the three-dimensional space, named ‘Pyramid’ (to be released in the near future, see <http://www.cs.berkeley.edu/~jrs>), may be utilized for our 3D CfCVDT generator.

## ACKNOWLEDGEMENTS

The authors would like to thank the unknown referees for their valuable comments which improved the paper a lot. The first author was partially supported by the National Science Foundation under grant number DMS-0609575 and the University of South Carolina Research and Productive Scholarship under grant number RPS-13060-06-12306. The second author was supported by Grant No. R01-2006-000-10472-0 from KOSEF.

## REFERENCES

1. Dörfler W. A convergent adaptive algorithm for Poisson’s equation. *SIAM Journal on Numerical Analysis* 1996; **33**:1106–1124.
2. Babuska I, Rheinboldt WC. Error estimates for adaptive finite element computations. *SIAM Journal on Numerical Analysis* 1978; **15**:736–754.
3. Babuska I, Rheinboldt WC. A posteriori error analysis of finite element solutions for one dimensional problems. *SIAM Journal on Numerical Analysis* 1981; **18**:565–589.
4. Arnica D, Padra C. A posteriori error estimators for the steady incompressible Navier–Stokes equations. *Numerical Methods for Partial Differential Equations* 1998; **13**:561–574.

## NUMERICAL SIMULATIONS OF THE STEADY NAVIER–STOKES EQUATIONS

5. Ainsworth M, Oden J. *A Posteriori Error Estimation in Finite Element Analysis*. Wiley: New York, 2002.
6. Oden JT, Wu W, Ainsworth M. An a posteriori error estimate for finite element approximations of the Navier–Stokes equations. *Computer Methods in Applied Mechanics and Engineering* 1994; **111**:185–202.
7. Morin P, Nochetto RH, Siebert KG. Data oscillation and convergence of adaptive FEM. *SIAM Journal on Numerical Analysis* 2000; **38**:466–488.
8. Morin P, Nochetto RH, Siebert KG. Local problems on stars: a posteriori error estimators, convergence, and performance. *Mathematics of Computation* 2003; **72**:1067–1097.
9. Verfurth R. A posteriori error estimates for non-linear problems: finite element discretizations of elliptic equations. *Mathematics of Computation* 1994; **62**:445–475.
10. Ju L, Gunzburger M, Zhao W-Z. Adaptive finite element methods for elliptic PDEs based on conforming centroidal Voronoi Delaunay triangulations. *SIAM Journal on Scientific Computing* 2006; **28**:2023–2053.
11. Temam R. *Navier–Stokes Equations*. North-Holland: Amsterdam, 1984.
12. Girault V, Raviart PA. *Finite Element Methods for Navier–Stokes Equations*. Springer: Berlin, 1986.
13. Ju L. Conforming centroidal Voronoi Delaunay triangulation for quality mesh generation. *International Journal for Numerical Analysis and Modelling* 2007; **4**:531–547.
14. Du Q, Faber V, Gunzburger M. Centroidal Voronoi tessellations: applications and algorithms. *SIAM Review* 1999; **41**:637–676.
15. Du Q, Gunzburger M. Grid generation and optimization based on centroidal Voronoi tessellations. *Applied Mathematics and Computation* 2002; **133**:591–607.
16. Du Q, Wang D. Tetrahedral mesh generation and optimization based on centroidal Voronoi tessellations. *International Journal for Numerical Methods in Engineering* 2003; **56**:1355–1373.
17. Du Q, Wang D. On the optimal centroidal Voronoi tessellations and the Gersho’s conjecture in the three-dimensional space. *Computer and Mathematics with Applications* 2005; **49**:1355–1373.
18. Gersho A, Gray R. *Vector Quantization and Signal Compression*. Kluwer: Boston, 1992.
19. Arya S, Mount D. Approximate nearest neighbor searching. *Proceedings of the 4th Annual ACM-SIAM Symposium on Discrete Algorithms (SODA’93)*, Austine, TX, U.S.A., 1993; 271–280.
20. Shewchuk J. *Triangle: Engineering a 2D Quality Mesh Generator and Delaunay Triangulator*. Lecture Notes in Computer Science, vol. 1148. Springer: New York, 1996; 203–222.